Nuclear Science and Techniques (2026) 37:22
https://doi.org/10.1007/s41365-025-01854-6

Linear relationship between reactivity and the reciprocal of uranium concentration in thermal-spectrum molten salt reactors

Chang-Qing Yu[1,2] · Gui-Feng Zhu[1,2] · Shu-Yang Jia[1,2] · Yang Zou[1,2] · Rui Yan[1,2] · Jian Guo[1,2] · Ya-Fen Liu[1,2] · Bo Zhou[1,2] · Xue-Chao Zhao[1,2] · Xiao-Han Yu[1,2]

Received: 17 December 2024 / Revised: 10 March 2025 / Accepted: 13 March 2025 / Published online: 3 January 2026

Abstract

Knowing the precise relationship between fuel loading and reactivity is essential for guiding reactor criticality extrapolation and online refueling in molten salt reactors (MSRs). This study aims to explore and explain the linear relationship between reactivity and the reciprocal of uranium concentration in thermal-spectrum MSRs. By applying neutron balance theory, we analyzed the neutron absorption cross sections of various nuclides in single-lattice models with varying fuel concentrations. Our findings reveal a simple linear correlation between reactivity and the reciprocal of uranium concentration, which can be explained from the perspective of nuclear reaction cross sections that adhere to the $1/v$ law in the thermal neutron spectrum. Furthermore, we identified that the neutron absorption single-group cross sections of structural materials and carrier salts exhibit an approximately linear relationship with the fission single-group cross section of ^{235}U; similarly, the reciprocal of ^{235}U's fission cross section exhibits an approximately linear relationship with uranium concentration. This linear relationship deviates as the volume fraction of molten salt increases, due to a greater proportion of neutrons being captured in the resonance energy spectrum. However, it remains valid for molten salt volume fractions up to 25% and demonstrates broad applicability in the physical design and operation of thermal molten salt reactors.

Keywords Molten salt reactor · Reactivity · Uranium concentration · Cross sections · Linear

1 Introduction

At the Generation IV International Forum (GIF), global experts on nuclear energy systems established a consensus on fourth-generation reactor technologies and ultimately selected six candidate designs [1, 2]. Among these, molten salt reactors (MSRs) stand out as the only liquid-fueled system, utilizing molten salt as both fuel and coolant [3–5]. This unique liquid fuel characteristic fundamentally distinguishes the fuel loading methodology from that of solid-fueled reactors, such as pressurized water reactors (PWRs) [6–8]. In PWRs, prefabricated fuel assemblies are loaded into the core in discrete batches with spatial heterogeneity intentionally introduced by varying the assembly types or structural configurations [9]. In salt reactors, nuclear fuel is typically introduced directly into the core and uniformly distributed throughout the fuel salt loop as the salt flows, without accounting for temperature distribution effects [10]. Monitoring reactivity variations during reactor loading is crucial for safety, and the liquid fuel characteristics in MSRs

This work was supported by the Youth Innovation Promotion Association of the Chinese Academy of Sciences (No. 2020261), the Strategic Priority Research Program of the Chinese Academy of Sciences (No. XDA02010000), the Young Potential Program of the Shanghai Institute of Applied Physics, Chinese Academy of Sciences (No. SINAP-YXJH-202412).

✉ Gui-Feng Zhu
zhuguifeng@sinap.ac.cn

✉ Yang Zou
zouyang@sinap.ac.cn

[1] State Key Laboratory of Thorium Energy, Shanghai Institute of Applied Physics, Chinese Academy of Science, Shanghai 201800, China

[2] University of Chinese Academy of Sciences, Beijing 100049, China

result in unique relationships between reactivity and fuel loading.

Liquid-fueled MSRs can be classified into two main types based on their neutron spectra: thermal-spectrum and fast-spectrum MSRs [11]. Thermal-spectrum MSRs typically employ graphite as a moderator and fluoride salts as the fuel salt [12, 13]. By contrast, fast-spectrum MSRs lack a moderator and can utilize either fluoride or chloride salts as fuel salts [14–16]. Additionally, there is a unique variant of MSRs that uses solid fuel while relying on liquid molten salt as the coolant [17, 18]. This design features fuel structures, such as coated particle fuel pebbles or fuel rods, with physical characteristics resembling those of traditional solid-fueled reactors. It is important to note that the scope of this study is focused exclusively on liquid-fueled MSRs and does not consider the solid fuel variant.

Research on MSRs can be traced back to the mid-twentieth century, with the most well-known example being the molten salt reactor experiment (MSRE). The MSRE achieved initial criticality on June 1, 1965, making it the longest operating MSR to date [19]. The initial loading process of the MSRE is summarized as follows: 4560 kg of carrier salt (64.75% LiF, 30.09% BeF_2, and 5.16% ZrF_4) and 236 kg of depleted uranium feed salt (73% LiF and 27% $^{238}UF_4$) were thoroughly mixed outside the reactor vessel and then transferred through piping into the reactor vessel. Subsequently, calculations indicated that a specific amount of highly enriched uranium feed salt (73% LiF, 27% UF_4, with ^{235}U at 93 wt%) was mixed in a similar manner outside the reactor vessel and then injected into the reactor vessel. This process was repeated until the extrapolated results indicated the need to add approximately 1 kg of highly enriched uranium fuel. Through the pump's feeding port, fuel capsules containing 150 g of highly enriched uranium feed salt (73% LiF, 27% UF_4, with ^{235}U at 93 wt%) were gradually introduced. After melting at high temperatures, the molten salt flowed out of the fuel capsule openings and was mixed with the fuel salt inside the reactor vessel, thereby completing the initial critical loading process [19, 20]. Throughout the feeding process, the nuclear fuel was rapidly and uniformly mixed into the fuel salt system, effectively increasing the uranium concentration within it.

Loading nuclear fuel and achieving initial reactor criticality are the most crucial steps prior to power operation, ensuring both safety and controllability. During the loading and criticality extrapolation processes, establishing the relationship between reactivity and the amount of nuclear fuel loaded serves as the physical basis for designing loading schemes. The reciprocal neutron count rate extrapolation method is commonly used to extrapolate critical loading [21]. In this method, the reciprocal of the neutron counting rate is plotted against the amount of nuclear fuel loaded; extrapolating the resulting curve to its intersection with the horizontal axis provides an estimate of the fuel loading required to achieve criticality. The physical principle underlying this method is based on source multiplication theory [22]. According to this theory, the effective neutron multiplication factor k_{eff} can be approximated as:

$$k_{\mathrm{eff}} = 1 - \frac{N_0}{N}, \tag{1}$$

where N_0 and N represent the count rate of the neutron detector before and after nuclear fuel is loaded into the reactor, respectively. As more nuclear fuel is loaded, the neutron count rate (N) increases. Consequently, as the reactor approaches criticality, k_{eff} approaches 1 while N tends toward infinity. The reciprocal extrapolation method approximates a linear relationship between k_{eff} and the fuel loading; however, the resulting curve typically exhibits concavity because this proportional relationship is a conservative approximation—namely, as fuel loading increases, the reactivity introduced per unit of fuel decreases. Although such conservative approximations are generally beneficial for ensuring reactor criticality safety, they can sometimes lead to disadvantageous assessments of the reactor status.

In nuclear reactor physics, particularly during startup, reactivity measurements serve as a primary means of characterizing the reactor's condition. Common methods for measuring reactivity include the source multiplication method [23, 24], the inverse kinetics method [25], and the period method [26]. Although these methods are applicable to liquid-fueled salt reactors as well, they face similar challenges. All of these methods require processing neutron signals captured by detectors to obtain reactivity parameters. Due to factors such as the influence of the external neutron source and the spatial effects of control rods, achieving precise measurements under subcritical conditions is difficult. Consequently, some researchers have employed complex correction methods based on theoretical calculations to enhance measurement precision [27, 28]. Determining a direct relationship between reactivity and nuclear fuel loading would facilitate calculating reactor reactivity solely based on the amount of fuel loaded.

Due to the liquid fuel characteristics of salt reactors, online refueling during operation is feasible [5, 29], which compensates for the decreased reactivity resulting from fuel burnup. Currently, the online refueling process is primarily simulated using coupled neutron transport and burnup codes. In such simulations, the nuclear fuel addition rate is typically adjusted to regulate k_{eff}. Common methods employed include the secant method [30] and linear approximations of k_{eff} with respect to burnup depth or fuel addition rate [31]. These methods generally require multiple iterations of neutron transport calculations to update the fuel feed rate.

Therefore, establishing a relationship between reactivity and nuclear fuel loading is crucial both for reactivity measurements and as a guiding principle for fuel loading, critical extrapolation, and criticality search calculations. It is widely recognized that reactivity and the amount of nuclear fuel loaded exhibit complex nonlinear relationships [32], making it difficult to establish a simple theoretical relationship. However, as noted earlier, the fuel loading process in a MSR primarily involves increasing the concentration of uranium (or another nuclear fuel) in the fuel salt without altering the reactor's structural configuration. Thus, under consistent operational conditions, a relationship should exist between the uranium concentration in the fuel salt and reactor reactivity. Building on this concept, our analysis of the relationship between k_{eff} and uranium concentration identified a highly linear correlation between reactivity and the reciprocal of uranium concentration. However, further investigations are required to explore the theoretical foundation and applicability of this linear relationship.

The objective of this study is to theoretically establish and validate the relationship between uranium concentration in MSR fuel salts and reactor reactivity, with particular emphasis on the underlying principles and applicability of the linear relationship. The remainder of this paper is organized as follows: Sect. 2 introduces the reactor model; Sect. 3 describes the discovery process of the linear relationship between $1/k_{\text{eff}}$ and the reciprocal of uranium concentration; Sect. 4 focuses on verifying the underlying principle through a step-by-step derivation based on a graphite-moderated single-lattice model and neutron balance theory, which explains the linear relationship between $1/k_{\text{eff}}$ and the reciprocal of uranium concentration; Sect. 5 verifies the applicability of the linear relationship using a graphite-moderated core model across a broader range of fuel loading conditions and scenarios involving different molten salt volume fractions (VFs), uranium enrichment levels, and ^{232}Th/^{233}U fuel; and finally, Sect. 6 summarizes and discusses the study's findings.

2 Reactor model

This study focuses on the relationship between reactor reactivity and uranium concentration in MSRs, using a graphite-moderated model as the basis of investigation. The reactor core employs graphite as a moderator and primarily consists of fuel salt channels, graphite moderators, graphite reflectors, and reactor vessels, as illustrated in Fig. 1. The lattice structure is hexagonal prismatic with a salt volume fraction of 15%, meaning that fuel salt occupies 15% of the total volume. The core active region measures 200 cm in both diameter and height. The moderator and reflector graphite have a density of 2.3 g/cm^3, and the reflector is 30 cm thick. The reactor was operated with a fuel salt composed of 67LiF-33BeF_2-xUF_4 (mol%). After adjusting the value of x, the fuel salt composition was normalized. Additionally, the fuel salt may include a certain proportion of ThF_4 to simulate thorium loading, which is further analyzed in Sect. 5.4. The density of the molten salts is calculated from the densities of the unit salts [33] using a volume-weighted average [34]. The accuracy of this method, based on the average molar volume, is within 3% [35]. The fuel salt parameters are listed in Table 1.

The theoretical analysis based on the single-lattice model, as well as its validation within the core model, was derived from simulations conducted using the CSAS6 module in

Table 1 Fuel salt parameters

Parameters	Value
Fuel salt (mol%)	67LiF-33BeF_2-xUF_4
Temperature	900 K
Salt density (g/cm^3)	LiF: $1.81 - 0.00049 \times (T - 848.2)$
	BeF_2: $1.96 - 0.000015 \times (T - 552)$
	UF_4: $6.485 - 0.00092 \times (T - 1036)$
	ThF_4: $6.058 - 0.000759 \times (T - 1110)$
^{7}Li abundance	99.95 at%
^{235}U enrichment	20 wt%

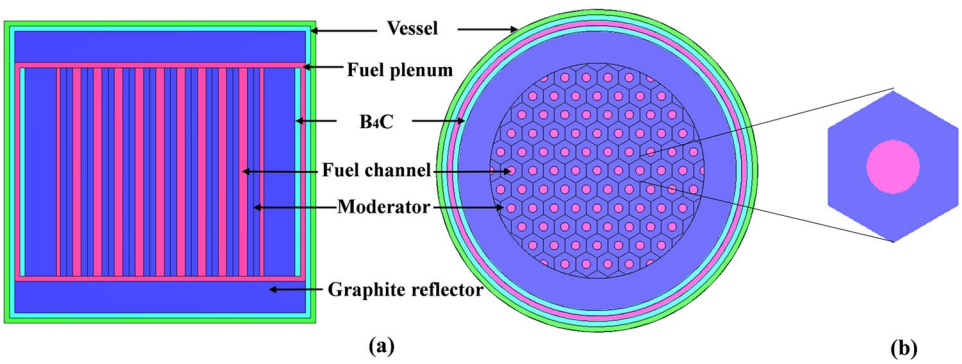

Fig. 1 (Color online) Schematic diagram of the (**a**) reactor core and (**b**) single-lattice models

SCALE6.1 [36]. The CSAS6 module combines a cross section processing module with a three-dimensional Monte Carlo transport code to perform a criticality analysis. Specifically, BONAMI is utilized to process cross sections in the unresolved resonance energy region, whereas CENTRM/PMC processes cross sections in the resolved resonance energy region. Transport calculations were performed using KENO-VI. CSAS6 provides critical outputs, such as k_{eff}, neutron energy spectra, and single-group cross sections for various fuel compositions. In this study, criticality calculations were performed with 20,000 particles, and the 238-group ENDF/B-VII.0 library was selected as the database.

3 The discovery of the linear relationship

Prior to the study presented in this paper, initial research focused on reactor loading and criticality extrapolation processes based on the reactor model illustrated in Fig. 1a. In particular, the study emphasized reactivity calculations during the loading process. As mentioned previously, the simulation incrementally increases the mole percentage of UF_4 in the fuel composition 67LiF-33BeF_2-$x$$UF_4$ (mol%), where x represents the amount of UF_4. Owing to the liquid fuel characteristics of the MSR, each batch of nuclear fuel is rapidly mixed and uniformly distributed throughout the fuel channel [37, 38]. Consequently, there is a direct relationship between reactor reactivity and the amount of fuel added, thereby eliminating the need to consider the spatial arrangement of the fuel, as is required in pressurized water reactors. Simulations using SCALE6.1 can determine k_{eff} after each batch of nuclear fuel is added, and efforts have been made to establish the relationship between the uranium concentration (or uranium loading) in the fuel salt and k_{eff}. During the extrapolation process for fuel addition, a practical approximation was employed under the assumption that the increase in k_{eff} is linearly related to the amount of fuel added. Therefore, the study initially analyzes the relationship between k_{eff} and the concentration of ^{235}U, as shown in Fig. 2a. Here, $M_{\text{U-235}}$ refers to the atomic number density of ^{235}U in the fuel salt (atoms/barn·cm). The relationship between k_{eff} and $M_{\text{U-235}}$ is concave and approximates linearity only when k_{eff} approaches 1.

To establish the relationship between k_{eff} and $M_{\text{U-235}}$, neutron balance theory was employed. According to this theory, the effective multiplication factor k_{eff} of a reactor system can be defined as the ratio of the neutron production rate to the neutron loss rate [39]

$$k_{\text{eff}} = \frac{\text{neutron production rate}}{\text{neutron loss rate(absorption + leakage)}}. \tag{2}$$

The effective multiplication factor is affected by material composition, reactor structure, and neutron leakage. A more detailed mathematical formulation is given by:

$$k_{\text{eff}} = \frac{\nu R_{\text{f}}}{R_{\text{a}} + L}. \tag{3}$$

In Eq. (3), ν represents the average number of neutrons emitted per fission; R_{f} is the fission reaction rate; R_{a} is the total absorption reaction rate, which includes contributions from the fuel salt, graphite, and structural materials; and L is the neutron leakage rate. Solving Eq. (3) requires determining the neutron flux and reaction cross sections through neutron transport calculations. Qualitatively, the uranium reaction rate is directly proportional to the concentration of ^{235}U. Furthermore, if one assumes that the neutron absorption

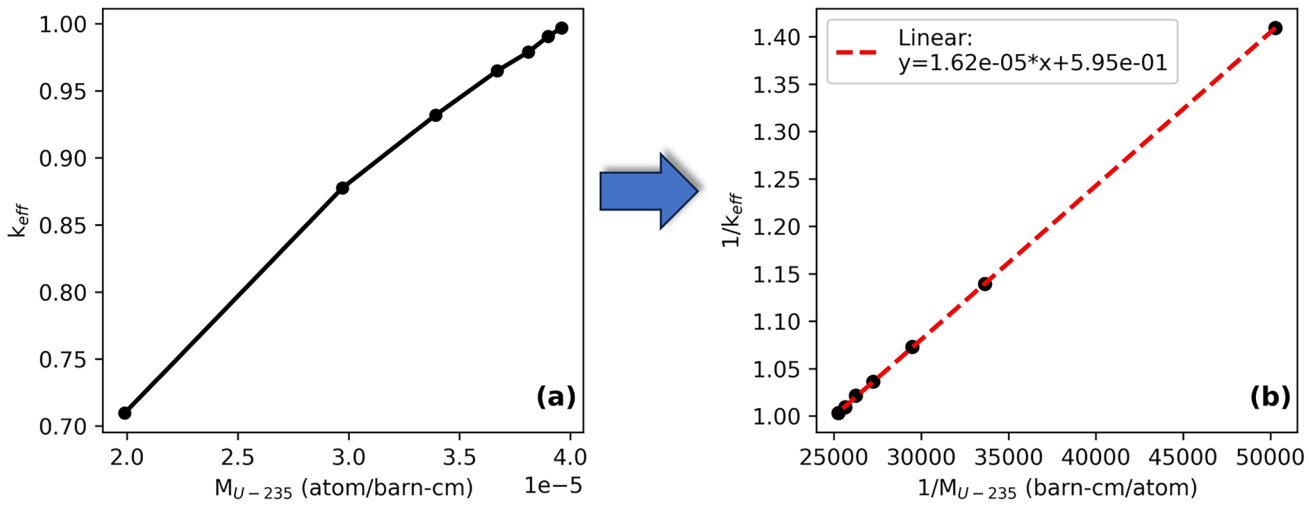

Fig. 2 (Color online) Relationship between k_{eff} and uranium concentration: the curve between k_{eff} and $M_{\text{U-235}}$ (**a**), and the linear relationship between $1/k_{\text{eff}}$ and $1/M_{\text{U-235}}$ (**b**)

reaction rate R_c for materials other than the uranium isotopes remains constant, then Eq. (3) can be approximated and rewritten as:

$$k_{\text{eff}} = \frac{c_{01} M_{\text{U-235}} \nu}{c_{02} M_{\text{U-235}} + R_c + L}, \tag{4}$$

where c_{01} and c_{02} are constants. By taking the reciprocal of both sides of Eq. (4) and assuming that ν and L are constant, the following form is obtained:

$$\frac{1}{k_{\text{eff}}} = a \cdot \frac{1}{M_{\text{U-235}}} + b. \tag{5}$$

Equation (5) suggests that $1/k_{\text{eff}}$ may exhibit an approximately linear relationship with $1/M_{\text{U-235}}$. To verify the validity of Eq. (5), Fig. 2a was modified by swapping the horizontal axis with $1/M_{\text{U-235}}$ and the vertical axis with $1/k_{\text{eff}}$, as shown in Fig. 2b. A linear fit of $1/k_{\text{eff}}$ versus $1/M_{\text{U-235}}$ yielded a determination coefficient (R^2) as high as 0.99997. Thus, although Eq. (5) is derived from the qualitative analysis of Eq. (3), the results shown in Fig. 2b confirm its validity. Equation (5) indicates that reactor reactivity can be quickly estimated based on uranium loading or concentration, which is advantageous for the reactor loading process.

Owing to the liquid fuel characteristics of salt reactors, loading nuclear fuel is equivalent to increasing the uranium concentration in the fuel salt. Based on the qualitative progression from Eq. (2) to Eq. (5) and the linear regression analysis shown in Fig. 2b, we found that reactor reactivity (or $1/k_{\text{eff}}$) exhibits a linear relationship with the reciprocal of the uranium concentration. However, in an actual fuel loading process, the neutron absorption reaction cross sections of various nuclides in the reactor may change, and the assumptions embedded in Eq. (4) (i.e., that c_{01}, c_{02}, and R_c are constant) may not hold perfectly. This observation necessitates further research.

Moving forward, this study utilizes neutron balance theory to examine the neutron energy spectrum and the variations in reaction cross sections as the uranium concentration changes. This approach progressively resolves Eq. (3) and provides a theoretical validation of the linear relationship proposed in Eq. (5).

4 Principle validation

To investigate the relationship between reactivity and uranium concentration using neutron balance theory, we utilized the single-lattice cell model illustrated in Fig. 1b. The hexagonal single-lattice model features a central channel for the fuel salt surrounded by a graphite moderator. This simplified model omits intricate core configurations, thereby eliminating the need to consider neutron absorption by structural materials [40, 41]. In addition, to neglect the influence of neutron leakage, a white reflective boundary condition was applied to the single-lattice structure. During calculations in SCALE 6.1, the concentration range of UF_4 was 0.02–1 mol%, corresponding to a k_{eff} range of 0.12−1.42, ensuring a sufficiently broad scope for analysis. Consequently, the neutron absorption reactions in Eq. (3) include only fuel salt and graphite moderator materials, with a leakage rate (L) of zero. The equation can be further expanded as

$$k_{\text{eff}} = \frac{\nu\left(\sigma_f^{\text{U-235}} M_{\text{U-235}} + \sigma_f^{\text{U-238}} M_{\text{U-238}}\right)}{\left(\sigma_a^{\text{U-235}} M_{\text{U-235}} + \sigma_a^{\text{U-238}} M_{\text{U-238}} + \sum \sigma_a^i M_i\right)}. \tag{6}$$

In Eq. (6), $\sigma_f^{\text{U-235}}$, $\sigma_f^{\text{U-238}}$, $\sigma_a^{\text{U-235}}$, and $\sigma_a^{\text{U-238}}$ denote the microscopic single-group cross sections for fission and absorption of ^{235}U and ^{238}U, respectively, while $M_{\text{U-235}}$ and $M_{\text{U-238}}$ represent their atomic number densities. The terms σ_a^i and M_i correspond to the single-group absorption cross sections and the atomic number densities of nuclides other than ^{235}U and ^{238}U, where i includes ^{6}Li, ^{7}Li, ^{9}Be, ^{19}F, and ^{12}C. Owing to the approximate proportionality between the average neutron flux density in the graphite moderation region and that in the fuel region, the single-group cross section of ^{12}C underwent treatment for neutron flux equivalence.

Careful observation of Eq. (6) shows that with an enrichment of 20 wt% for ^{235}U there is a fixed proportional relationship between $M_{\text{U-235}}$ and $M_{\text{U-238}}$. In addition, during the fuel loading process, variations in the concentrations of nuclides other than uranium can be considered negligible. Moreover, because the fissile material (uranium) has fixed enrichment, the average number of fission neutrons (ν) can be approximated as constant. Therefore, the primary variables on the right-hand side of Eq. (6) are the single-group cross sections of each nuclide and the uranium concentration. Next, we examined the variation in single-group cross sections with uranium concentration, incorporating the neutron energy spectrum, and gradually simplified Eq. (6).

4.1 Variations in energy spectrum and cross sections

The single-group cross sections are primarily determined by the neutron energy spectrum and are calculated as follows:

$$\bar{\sigma} = \frac{\int \sigma(E)\phi(E)\,\mathrm{d}E}{\int \phi(E)\,\mathrm{d}E}, \tag{7}$$

where $\sigma(E)$ represents the nuclear reaction cross section at energy E (which remains fixed for a given nuclide and reaction type) and $\phi(E)$ represents the neutron flux distribution in the region where the nuclide is present. The neutron energy spectrum is influenced by the reactor structure, uranium

concentration, and temperature. Neutron transport calculations using SCALE 6.1 are used to determine this spectrum.

Figure 3a shows the normalized neutron energy spectra in the fuel region at different uranium concentrations, along with the cross sections of the key neutron absorption reactions in a single lattice. For fissile isotopes, the primary neutron absorption reactions of ^{235}U and ^{238}U are the fission (n, f) and capture (n, γ) reactions. For ^{6}Li, the primary reaction is tritium production via the (n, T) reaction. The dominant nuclear reaction type for other light nuclei is the capture absorption (n, γ) reaction. Additionally, for the nuclides ^{9}Be and ^{19}F, a significant proportion of the absorption occurs via (n, α) reactions in the high-energy region, where neutrons are absorbed to produce ^{4}He particles. It is noted that although the neutron flux in the thermal energy region ($E < 1$ eV) decreases with increasing uranium concentration, there is a corresponding increase in other energy regions. However, overall, the thermal region remains significantly dominant compared to the fast neutron region, indicating a predominantly thermal spectrum. Furthermore, although the neutron flux in different energy regions varies with uranium concentration, the overall characteristics of the spectrum's shape remain essentially unchanged. Observe the variation in reaction cross sections for major nuclides with energy in Fig. 3a. For the two fissile nuclides ^{235}U and ^{238}U, both their fission and capture cross sections in the thermal region follow the $1/v$ law (i.e., $\sigma(E) \propto 1/\sqrt{E}$), and v is the neutron velocity. In the intermediate-energy region, strong resonance peaks occur—particularly for ^{238}U. In contrast, the neutron absorption cross sections of other light nuclei, except for the ^{9}Be(n, α) and ^{19}F(n, α) reactions, follow the $1/v$ law over a wider energy range.

Based on the analysis of the neutron energy spectrum and neutron absorption reaction cross sections, three main observations can be made:

1. The neutron energy spectrum is thermal, with the thermal neutron flux ($E < 1$ eV) significantly higher than the flux at other energies.
2. The neutron absorption cross sections of major nuclides in the thermal region follow the $1/v$ law (i.e., $\sigma(E) \propto 1/\sqrt{E}$).
3. In the high-energy neutron range, isotopes such as ^{235}U, ^{238}U, and ^{19}F exhibit prominent resonance absorption peaks. Moreover, ^{9}Be and ^{19}F also have significant (n, α) absorption cross sections in the fast neutron energy region.

Based on these three observations and Eq. (7), we can qualitatively infer that the single-group neutron absorption cross sections of the major nuclides may exhibit an approximately linear relationship with the single-group fission cross section of ^{235}U. However, owing to the strong resonance absorption peaks in isotopes such as ^{235}U and ^{238}U, as well as the (n, α) reactions in ^{9}Be and ^{19}F, deviations from strict linearity may occur. To further illustrate this issue, Fig. 3b shows the normalized neutron reaction rate versus the energy distribution for the major nuclides under critical conditions with uranium comprising 0.36 mol%. Figure 3b shows that in the thermal energy region ($E < 1$ eV), the neutron reaction rates of the major nuclides are ranked as follows: ^{235}U$(n, \alpha) > ^{235}$U$(n, f) > ^{6}$Li$(n, \alpha) > ^{12}$C$(n, \alpha) > ^{7}$Li$(n, \alpha) > ^{19}$F$(n, \alpha) > ^{238}$U$(n, \alpha) > ^{9}$Be(n, α). For major nuclides such as ^{235}U, ^{6}Li, ^{12}C, and ^{7}Li, the neutron absorption reaction rates in the thermal region are significantly higher than those in other energy regions. When calculating k_{eff} via Eq. (6), it is therefore essential to primarily consider the neutron reaction

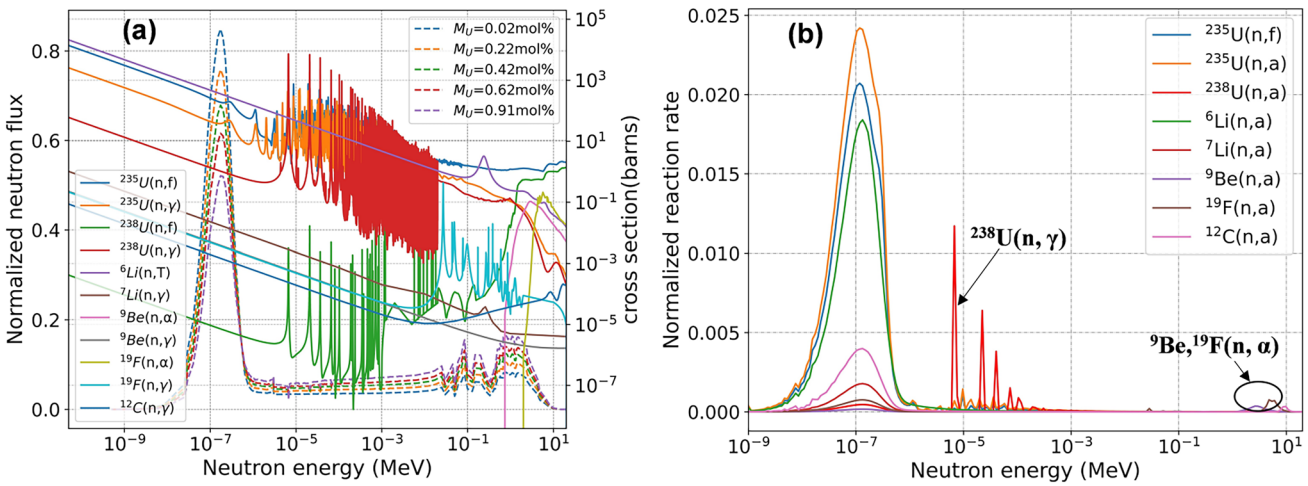

Fig. 3 (Color online) Neutron energy spectrum and cross sections of major nuclides (**a**), distribution of normalized reaction rates with energy (**b**)

rates in the thermal region. In the resonance energy region, both ^{238}U and ^{235}U undergo significant absorption reactions. For ^{238}U, resonant absorption in the energy range of 1 eV–1 keV constitutes approximately 75% of its total absorption; however, this comprises only about 2% of the overall material absorption. In addition, due to the (n, α) reactions of ^{9}Be and ^{19}F, these nuclides exhibit a notable fraction of their neutron absorption in the fast region—approximately 45% and 19% of their total absorption, respectively. However, these rates are significantly lower than the absorption reaction rates of nuclides such as ^{235}U and ^{6}Li in the thermal region. Therefore, for nuclides that contribute significantly to neutron absorption reactivity, the focus is primarily on thermal absorption reactions, in which the cross sections follow the $1/v$ law. Although some nuclides also contribute in the resonance and fast regions, their contributions remain relatively small.

To verify the above analysis, we used SCALE 6.1 to calculate the single-group neutron absorption cross sections for the major nuclides and examined their linear relationships with the ^{235}U fission cross section. Figure 4 shows the linear relationship between the single-group absorption cross sections of ^{235}U, ^{238}U, ^{6}Li, ^{7}Li, ^{9}Be, ^{19}F, and ^{12}C versus the single-group fission cross section of ^{235}U. The corresponding coefficient of determination (R^2) for each linear fit is provided. As Fig. 4 demonstrates, the neutron absorption cross sections of various nuclides exhibit a strong linear relationship with the fission cross section of ^{235}U. This linear relationship can be expressed as:

$$\sigma_{\mathrm{a}}^{i} = c_1^{i}\sigma_{\mathrm{f}}^{\mathrm{U-235}} + c_2^{i}, \tag{8}$$

where σ_{a}^{i} represents the single-group neutron absorption cross section of nuclide i, $\sigma_{\mathrm{f}}^{\mathrm{U-235}}$ denotes the single-group fission cross section of ^{235}U, and c_1^{i} and c_2^{i} are the slope and intercept of the linear fit for nuclide i, with i including ^{235}U, ^{238}U, ^{6}Li, ^{7}Li, ^{9}Be, ^{19}F, and ^{12}C. Figure 4 shows that the coefficients of determination (R^2) for ^{238}U and ^{9}Be are relatively small. This is primarily due to the strong resonance absorption peak of ^{238}U in the intermediate-energy region and the relatively large (n, α) absorption cross section of ^{9}Be in the fast region, as shown in Fig. 3a or b. An increase in uranium concentration results in a harder neutron energy spectrum, enhancing both resonance and (n, α) absorption, which leads to deviations from strict linearity. However, because the single-group absorption cross sections of these nuclides are significantly smaller than those of major nuclides (such as ^{235}U and ^{6}Li), using Eq. (8) as a linear approximation does not significantly affect the calculation of k_{eff} in Eq. (6).

Thus, we can convert all the single-group absorption cross sections in Eq. (6) into expressions based on the fission cross section of ^{235}U. Accordingly, Eq. (6) can be simplified further to

$$k_{\mathrm{eff}} = \frac{\nu(\sigma_{\mathrm{f}}^{\mathrm{U-235}}M_{\mathrm{U\text{-}235}} + \sigma_{\mathrm{f}}^{\mathrm{U-238}}M_{\mathrm{U\text{-}238}})}{(c_1^{\mathrm{U-235}} + wc_1^{\mathrm{U-238}})\sigma_{\mathrm{f}}^{\mathrm{U-235}}M_{\mathrm{U\text{-}235}} + \sum c_1^{i}M_i\sigma_{\mathrm{f}}^{\mathrm{U-235}} + (c_2^{\mathrm{U-235}} + c_2^{\mathrm{U-238}}w)M_{\mathrm{U\text{-}235}} + \sum c_2^{i}M_i},$$
$$w = \frac{(1-wt)\times 235}{wt\times 238}, \tag{9}$$

where wt.% represents the enrichment of ^{235}U. Meanwhile, as shown in Fig. 3a, the fission cross section of ^{238}U is four orders of magnitude lower than that of ^{235}U, so it is reasonable to neglect the contribution of ^{238}U's fission. Moreover, compared with $\sigma_{\mathrm{f}}^{\mathrm{U-235}}$, the intercepts of the linear fits of the absorption cross sections for ^{235}U and ^{238}U amount to only about 1% of $\sigma_{\mathrm{f}}^{\mathrm{U-235}}$ and can be neglected. Therefore, the absorption cross sections of ^{235}U and ^{238}U are approximately proportional to $\sigma_{\mathrm{f}}^{\mathrm{U-235}}$, and Eq. (9) can be further simplified to

$$k_{\mathrm{eff}} = \frac{\nu\sigma_{\mathrm{f}}^{\mathrm{U-235}}M_{\mathrm{U\text{-}235}}}{(c_1^{\mathrm{U-235}} + wc_1^{\mathrm{U-238}})\sigma_{\mathrm{f}}^{\mathrm{U-235}}M_{\mathrm{U\text{-}235}} + \sum c_1^{i}M_i\sigma_{\mathrm{f}}^{\mathrm{U-235}} + \sum c_2^{i}M_i}. \tag{10}$$

In Eq. (10), the slopes c_1^{i} and intercepts c_2^{i} associated with the linear fits for i (including ^{235}U, ^{238}U, and the other nuclides) as well as M_i are constants. Thus, k_{eff} has been simplified to depend solely on the fission cross section $\sigma_{\mathrm{f}}^{\mathrm{U-235}}$ of ^{235}U and its concentration $M_{\mathrm{U\text{-}235}}$. Next, we analyze the relationship between the fission cross section $\sigma_{\mathrm{f}}^{\mathrm{U-235}}$ and the uranium concentration $M_{\mathrm{U\text{-}235}}$ to further streamline Eq. (10).

4.2 Relationship between fission cross section and uranium concentration

In Eq. (6), k_{eff} is expressed as a function of cross sections and nuclide concentrations. Using Eq. (8), we established a relationship between the neutron absorption cross sections of the various nuclides and the fission cross section of ^{235}U. Consequently, if the concentration of nonfissile nuclides remains approximately constant, there are two quantities on the right-hand side of Eq. (10) that depend on k_{eff}, namely $M_{\mathrm{U\text{-}235}}$ and $\sigma_{\mathrm{f}}^{\mathrm{U-235}}$. Next, we establish the relationship between $M_{\mathrm{U\text{-}235}}$ and $\sigma_{\mathrm{f}}^{\mathrm{U-235}}$.

From Eq. (7), the calculation of the single-group cross section is directly related to the neutron spectrum; thus,

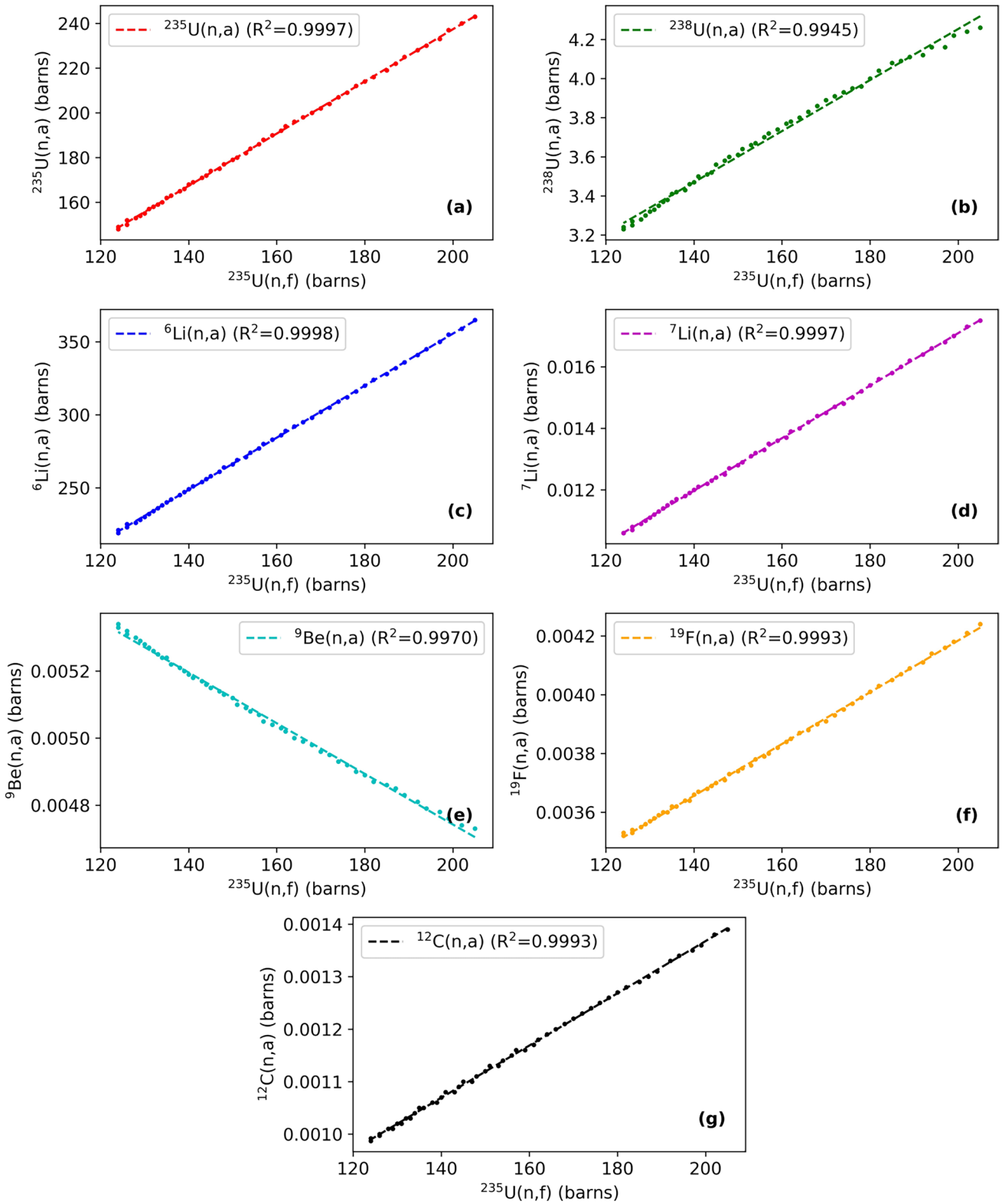

Fig. 4 (Color online) Linear fit of neutron absorption cross sections in major nuclides to the ^{235}U fission cross section

the spectrum governs the magnitude of the cross section. Furthermore, variations in the spectrum are primarily driven by fuel loading, underscoring the intrinsic link between the spectrum and uranium concentration. As the uranium concentration increases, neutron absorption strengthens, diminishing the moderator capacity of the fuel salt and resulting in spectrum hardening, as shown in Fig. 3a. Establishing an explicit relationship between the neutron spectrum and uranium concentration is challenging because it requires solving for the spectrum. Under the free gas model, the neutron spectrum follows a Maxwell–Boltzmann distribution. However, due to the continuous generation of fission neutrons and their subsequent absorption during moderation, the neutron spectrum shifts toward higher energies [42]. The present approach avoids seeking an analytical solution for the energy spectrum; instead, Eq. (7) is applied to determine the fission cross section, with neutron transport calculations directly providing the energy spectrum. Single-group cross sections are then processed to establish their relationship with uranium concentration using SCALE 6.1. A fitting analysis was conducted to examine the relationship between $\sigma_{\mathrm{f}}^{\mathrm{U\text{-}235}}$ and $M_{\mathrm{U\text{-}235}}$, and the results indicated that $1/\sigma_{\mathrm{f}}^{\mathrm{U\text{-}235}}$ and $M_{\mathrm{U\text{-}235}}$ exhibit a highly linear relationship, with a linear determination coefficient R^2 as high as 0.99998. This linear relationship can be expressed as

$$\frac{1}{\sigma_{\mathrm{f}}^{\mathrm{U\text{-}235}}} = c_3 M_{\mathrm{U\text{-}235}} + c_4, \tag{11}$$

where c_3 and c_4 are the slope and intercept of the linear fit, respectively, and are constants. The results of the linear fitting are shown in Fig. 5. Qualitatively, as $M_{\mathrm{U\text{-}235}}$ increases, the neutron spectrum hardens and the single-group fission cross section decreases. This linear relationship may be related to the $1/v$ law that governs the fission cross section in the thermal neutron region, although further theoretical exploration based on the energy spectrum is required.

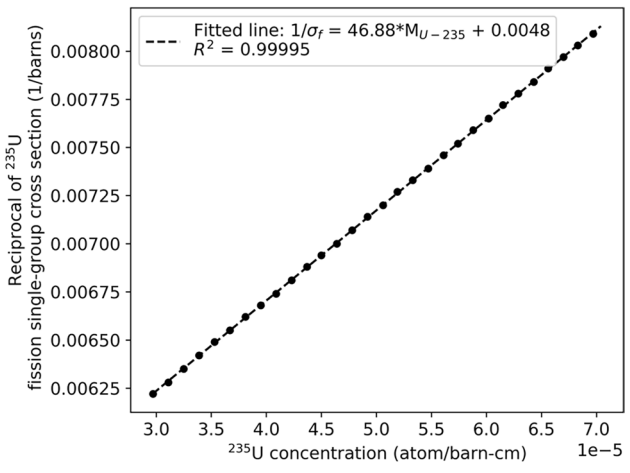

Fig. 5 (Color online) Linear fit of the reciprocal of the ^{235}U fission cross section with concentration

Substituting Eq. (11) into Eq. (10) allows further simplification, yielding

$$\begin{aligned} k_{\mathrm{eff}} &= \frac{M_{\mathrm{U\text{-}235}}}{a + bM_{\mathrm{U\text{-}235}}}, \\ a &= \left(\sum c_1^i M_i - c_4 \sum c_2^i M_i\right)/\nu, \\ b &= \left(c_3 \sum c_2^i M_i + c_1^{\mathrm{U-235}} + w c_1^{\mathrm{U-238}}\right)/\nu. \end{aligned} \tag{12}$$

In Eq. (12), k_{eff} depends solely on the concentration of ^{235}U. Taking the reciprocal of both sides of Eq. (12) leads to Eq. (5), demonstrating that $1/k_{\mathrm{eff}}$ (or reactivity, defined as $\rho = 1 - 1/k_{\mathrm{eff}}$) is linearly related to the reciprocal of uranium concentration. From this, it is evident that the slope and intercept, a and b, of the linear relationship between reactivity and the reciprocal of $M_{\mathrm{U\text{-}235}}$ are mainly determined by the linear relationships between the cross sections (embodied in c_1^i and c_2^i) and the linear relationship between $1/\sigma_{\mathrm{f}}^{\mathrm{U\text{-}235}}$ and $M_{\mathrm{U\text{-}235}}$ (given by c_3 and c_4). In other words, the linear relationship expressed in Eq. (8), along with those in Eq. (12) and Eq. (5), is substantiated.

It can be observed from the derivation from Eq. (6) to Eq. (2) that several approximations have been employed. These approximations are summarized as follows:

1. The single-group absorption cross section of the main nuclide is linearly related to the single-group fission cross section of ^{235}U, as shown in Fig. 4 or Eq. (8). In other words, the absorption cross sections of ^{235}U and ^{238}U are approximately proportional to the ^{235}U fission cross section.
2. $1/\sigma_{\mathrm{f}}^{\mathrm{U\text{-}235}}$ exhibits a linear relationship with $M_{\mathrm{U\text{-}235}}$, as shown in Fig. 5 or Eq. (11).
3. The contribution from ^{238}U fission is excluded.
4. Changes in the concentrations of nuclides other than uranium are neglected.
5. The average number of neutrons per fission, ν, is assumed constant.

5 Validation of applicability

In the previous section, the single-lattice model shown in Fig. 1b was used to validate Eq. (5). By analyzing the variation in the single-group cross sections with changes in uranium concentration and applying reasonable approximations, we successfully demonstrated a linear relationship between reactivity and the reciprocal of the uranium concentration.

However, as shown in Fig. 1a, a typical reactor core structure includes not only an active core region but also reflector layers and various structural materials. These additional materials absorb neutrons to varying degrees and alter the neutron energy spectrum. Nevertheless, because these structures remain unchanged as the uranium concentration varies, they can be considered, from a physical standpoint, equivalent to a graphite moderation structure. Therefore, Eq. (5) (or Eq. (12)) remains valid for the core model. To validate this conclusion, we simulated and computed the variation in k_{eff} with uranium concentration using the core model.

5.1 Verification of the linear relationship

Based on the core model shown in Fig. 1a, we verified the linear relationship between $1/k_{\text{eff}}$ and $1/M_{\text{U-235}}$ under the condition that the volume fraction (VF) and the uranium enrichment (wt) of the molten salt channel in the single-lattice model are identical (i.e., VF = 15% and wt = 20%). Simultaneously, the uranium concentration was expanded from 0.02–1 mol% to 0.02–3 mol%. This section demonstrates the applicability of the aforementioned linear relationships to the core model.

The method involves using SCALE6.1 to calculate the k_{eff} of the reactor at different uranium concentrations and establishing the relationship between reactivity and uranium concentration. As shown in Fig. 6a, $1/k_{\text{eff}}$ exhibits a highly linear relationship with the reciprocal of uranium concentration (i.e., $1/M_{\text{U-235}}$). The fitted coefficient of determination, R^2, was 0.99995. Furthermore, with ^{235}U concentrations ranging from 1.4×10^{-6} to 2.0×10^{-4} atoms/barn·cm, the k_{eff} values span from 0.08 to 1.43, covering nearly all possible fuel loading scenarios. This verified the conclusion that the reactivity derived from the single-lattice model is linearly related to the reciprocal of the uranium concentration.

To further illustrate the accuracy of this linear relationship, Fig. 6b presents the statistical error in calculating k_{eff} directly using the SCALE6.1 program, as well as the relative deviation between k_{eff} derived from the linear relationship in Fig. 6a and the results calculated using SCALE6.1. Figure 6b shows that the error in calculating k_{eff} with SCALE6.1 is maintained between approximately 30 and 50 pcm. Although the relative deviation between k_{eff} calculated using the linear relationship and that from SCALE6.1 fluctuates more significantly, within the range of k_{eff} from 0.7 to 1.1 the deviation remains essentially within ±100 pcm. Therefore, Fig. 6b directly demonstrates the accuracy of calculating k_{eff} using the linear relationships shown in Fig. 6a within the allowable error range.

5.2 Impact of molten salt volume fraction (VF)

In deriving the linear relationship, the most important approximation is that the neutron absorption cross sections of all nuclides are linearly related to the fission cross section of ^{235}U (approximation condition (1)). The rationale for this approximation is that in graphite-moderated salt reactors the neutron energy spectrum is thermal, which diminishes the impact of resonance and fast neutron absorption reactions. When the fuel composition is unchanged, the neutron spectrum is primarily influenced by the proportion of molten salt in the graphite channels. This section discusses the applicability of the aforementioned linear relationships under different volume fraction (VF) conditions. The verification method involves maintaining a constant enrichment of ^{235}U at 20 wt% and calculating the relationship between k_{eff} and uranium concentration at different VFs using SCALE6.1, with VF ranging from 5% to 40%.

First, we observed how the neutron energy spectrum changes as VF varies. Figure 7 shows the normalized neutron

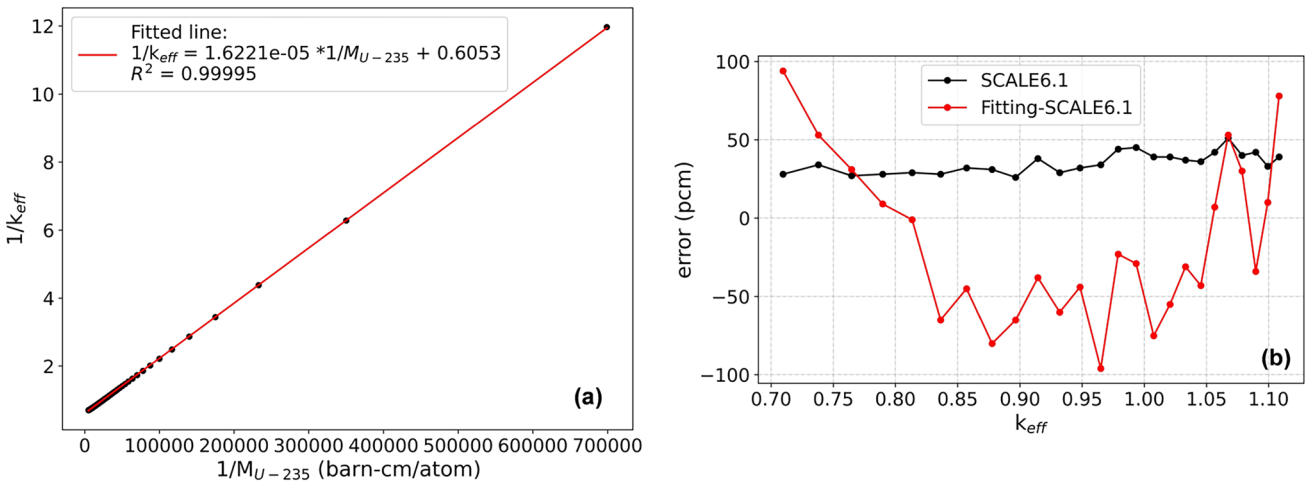

Fig. 6 (Color online) Linear relationship between $1/k_{\text{eff}}$ and $1/\text{M}_{\text{U-235}}$(**a**), accuracy of k_{eff} calculated by linear regression(**b**)

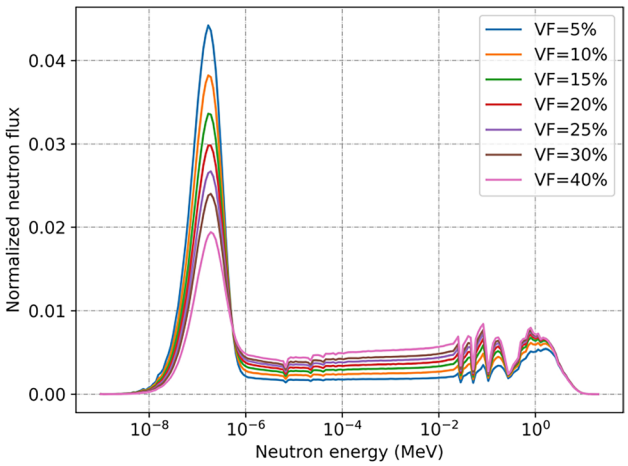

Fig. 7 (Color online) Normalized neutron energy spectrum at different volume fractions (VF)

flux distribution as a function of energy for different VF values. At each VF and with a constant uranium loading, the corresponding concentration of ^{235}U was 3.81×10^{-05} atoms/barn·cm. For $VF = 15\%$, $k_{\text{eff}} = 1$. Figure 7 indicates that the neutron energy spectrum undergoes significant changes as VF varies. The main effect is that, with increasing VF, the neutron flux decreases in the thermal region ($E < 1$ eV), while it increases in the intermediate-energy and fast neutron energy regions. Combining these changes with the neutron absorption cross sections from Fig. 3a, it becomes apparent that a relative increase in the neutron flux in the resonance or fast regions leads to a decrease in the fraction of neutrons that follow the $1/v$ law. As a result, the linearity between the absorption cross sections and the fission cross section of ^{235}U degrades, meaning that approximation condition (1) no longer holds perfectly. Ultimately, this causes a deviation from the linear relationship between reactivity and $1/M_{\text{U-235}}$.

Figure 8a shows the local curves of the relationship between $1/k_{\text{eff}}$ and $1/M_{\text{U-235}}$ for different VF values. As

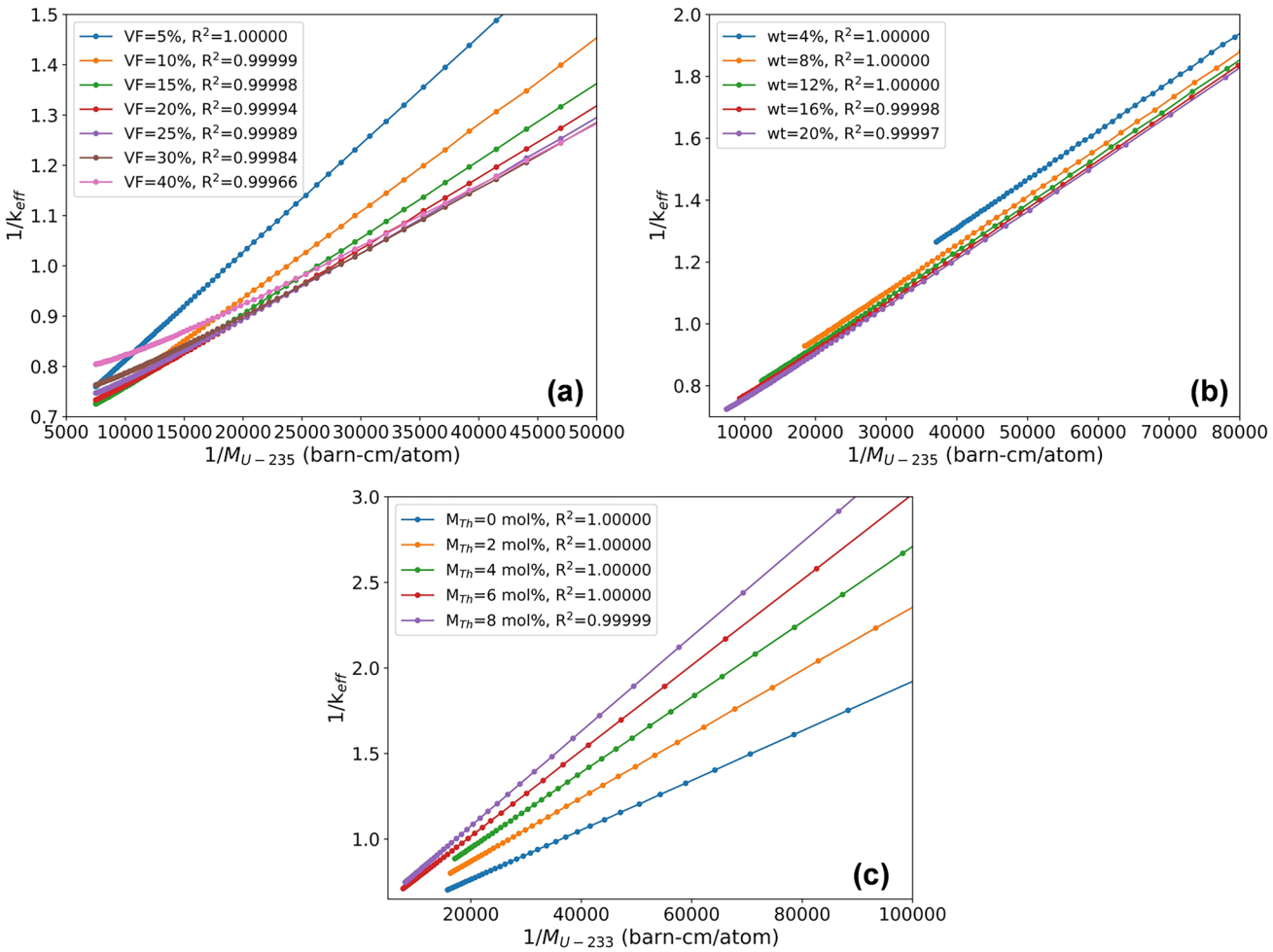

Fig. 8 (Color online) Relationship curves of $1/k_{\text{eff}}$ versus $1/M_{\text{U-235}}$ at different volume fractions (**a**), different uranium enrichments(**b**), different thorium loads(c)

VF increases, the curve gradually bends, with a more pronounced bend at higher VF values. Correspondingly, the determination coefficient (R^2) of the linear fit between $1/k_{\text{eff}}$ and $1/M_{\text{U-235}}$ gradually decreases, indicating increasing deviation from linearity. Figure 8a directly illustrates that an increase in VF—or equivalently, a hardening of the neutron spectrum—leads to deviation from the linear relationship between reactivity and the reciprocal of the uranium concentration. This deviation is gradual with VF, and the applicability of the linear relationship does not have a strict limit but is mainly related to the error requirements. In general, for a graphite-moderated MSR, the optimal design range for VF is 10–20% [40, 43, 44]. Within this range, the determination coefficient remains greater than 0.9999, indicating a highly linear relationship.

5.3 Impact of uranium enrichment

As shown in Fig. 3a, ^{238}U exhibits strong resonance capture cross sections, and its varying content in the fuel salt may result in different relationships between reactivity and uranium concentration. To validate the applicability of the linear relationship in Eq. (3) under various uranium enrichments, we examined the relationship between reactor reactivity and uranium concentration under different enrichments. The verification method involved keeping VF constant at 15% and using SCALE6.1 to calculate the relationship between k_{eff} and uranium concentration under different ^{235}U enrichments. In this study, the enrichment of ^{235}U in UF_4 ranged from 4 to 20 wt%, and the effect of enrichment variation on the density of UF_4 was neglected.

Figure 8b shows the relationship between $1/k_{\text{eff}}$ and the reciprocal of uranium concentration at different enrichments, along with the determination coefficient (R^2) obtained from linear fitting. It is evident that within the range of 4–20 wt% uranium enrichment, a strong linear correlation exists between $1/k_{\text{eff}}$ and $1/M_{\text{U-235}}$ with no deviation from linearity, as shown in Fig. 8a. The linear correlation coefficients for different enrichments are greater than 0.99995, demonstrating the applicability of this linear relationship across various enrichment conditions. Although the determination coefficients exhibit slight fluctuations, all values exceed 0.99995, indicating that these fluctuations are within the computational precision of the linear fitting and can be attributed to calculation errors. Therefore, we conclude that under various low-enriched uranium conditions, a strong linear relationship exists between reactor reactivity and the reciprocal of uranium concentration. Despite several-fold variations in uranium enrichment, the overall absorption cross section of ^{238}U remains much smaller than the fission cross section of ^{235}U [45]. Thus, changes in enrichment do not significantly affect the calculation of k_{eff} using Eq. (6). In contrast, variations in VF have a more pronounced impact by altering the neutron spectrum and affecting the absorption cross sections of all isotopes, including ^{238}U. Consequently, when VF becomes too large, nonlinear deviations from the linear relationship occur. In addition, the comparison of Figs. 8a and b reveals that, while the intercept of the linear fit varies with uranium enrichment, the slope remains nearly constant. However, at different VF values, both the intercept and slope change. This can be explained by Eq. (12): when uranium enrichment changes, the neutron energy spectrum varies only slightly; therefore, the coefficients c_i do not change significantly and the slope remains relatively stable, whereas the intercept, which is related to enrichment, changes accordingly.

5.4 ^{232}Th/^{233}U fuel

Based on the analysis of ^{235}U/^{238}U fuel, the primary reason for the linear relationship between reactor reactivity and the reciprocal of uranium concentration is that, in the thermal neutron energy region, the neutron absorption cross sections of the main nuclides follow the $1/v$ law. The fission cross section of ^{233}U is similar to that of ^{235}U and also adheres to the $1/v$ law. Therefore, the same linear relationship observed in the previous analysis should also apply to ^{232}Th/^{233}U fuel. To verify this conclusion, we examined the relationship between reactor reactivity and uranium concentration for ^{232}Th/^{233}U fuel. In this case, the core model is shown in Fig. 1a, and the fuel salt composition was 67LiF-33BeF_2-(0–8)ThF_4-xUF_4 (mol%). The ThF_4 content ranged from 0 to 8 mol% to validate the applicability of the linear relationship under different thorium loading conditions. Reactivity was adjusted by varying the amount of UF_4 (i.e., the value of x) under different thorium loadings. The verification results shown in Fig. 8c demonstrate that $1/k_{\text{eff}}$ and $1/M_{\text{U-233}}$ exhibit strong linear relationships under different thorium loadings. This confirms the applicability of the linear relationship to ^{232}Th/^{233}U fuel.

6 Conclusion

Owing to its liquid fuel characteristics, the graphite-moderated MSR treats the fuel loading process as equivalent to increasing the uranium concentration in the fuel salt. A corresponding relationship exists among uranium loading, concentration, and reactivity. This study first investigated the variation in the neutron spectrum and reaction cross sections with uranium concentration using a single-lattice cell model. Under certain approximations, a linear relationship was derived between reactor reactivity and the reciprocal of uranium concentration based on neutron balance theory. Subsequently, the applicability of this linear relationship was validated through simulation calculations using the core

model. Based on these studies, the following conclusions were drawn:

1. Due to the thermal neutron spectrum in graphite-moderated MSRs and the fact that, at low energies, the neutron absorption cross sections of various nuclides follow the 1/*v* law, the single-group neutron absorption cross sections of each nuclide approximately exhibit a linear relationship with the single-group fission cross section of ^{235}U.
2. The reciprocal of the ^{235}U single-group fission cross section is linearly related to the uranium concentration.
3. Based on the two premises above, the reactor reactivity is linearly related to the reciprocal of uranium concentration, being this the main conclusion of this study.
4. The linear relationship weakens as the volume fraction of graphite molten salt channels increases. However, within the optimal design range of VF = 10–20%, the coefficient of determination for this linear relationship remains greater than 0.9999, indicating a high degree of linearity.
5. The linear relationship is minimally affected by uranium ^{235}U enrichment in the range of 4–20 wt%. At VF = 15%, the coefficient of determination remains above 0.99995 across different enrichments, demonstrating a highly linear relationship.
6. For ^{232}Th/^{233}U fuel, this linear relationship also holds.

The relationship between reactor reactivity and nuclear fuel loading is generally considered complex. Typically, when nuclear fuel loading changes, complex neutron transport calculations must be performed to determine the impact on reactivity, which is both time-consuming and labor-intensive. Moreover, during the fuel loading process in experiments, reactors are often in a subcritical or deep subcritical state, further complicating reactivity measurements. This study established a simple relationship between reactivity and uranium concentration through simulation analysis, which can be used to calculate or measure reactor reactivity. Furthermore, the analysis effectively links the amount of nuclear fuel loaded to the corresponding reactivity, a relationship that is applicable in various scenarios, such as critical extrapolation during the fuel loading process. In summary, this study established a simple linear relationship between reactor reactivity and uranium concentration through theoretical analysis and simulation verification. This relationship has significant application value in both theoretical and experimental studies on MSRs. It should be noted that the reactor model used in this study had a single-zone structure (i.e., all lattices shared the same VF); for salt reactors with more complex partition designs, the relationship between reactivity and uranium concentration may take different forms and requires further validation.

Acknowledgements Thanks to the Chinese Academy of Sciences and all sectors of society for their support in the development of MSRs.

Author Contributions Chang-Qing Yu conceived and wrote the article, and performed the data analysis. Gui-Feng Zhu contributed to the funding, conceptualization, and writing. Shu-Yang Jia made significant contributions to the revision of the article. Zou Yang, Rui Yan, Jian Guo, Ya-Fen Liu, Bo Zhou, Xue-Chao Zhao, and Xiao-Han Yu provided suggestions for the analysis and assisted with revising the manuscript.

Data Availability The data that support the findings of this study are openly available in Science Data Bank at https://cstr.cn/31253.11.sciencedb.j00186.00750 and https://doi.org/10.57760/sciencedb.j00186.00750.

Declarations

Conflict of interest The authors declare that they have no conflict of interest.

References

1. A Technology Roadmap for Generation IV Nuclear Energy Systems Executive Summary. United States: DOENE, (2003). https://doi.org/10.2172/859105
2. T. Schulenberg, *The fourth generation of nuclear reactors: Fundamentals, Types, and Benefits Explained* (Springer Berlin Heidelberg, Berlin, 2022), pp. 147–165. https://doi.org/10.1007/978-3-662-64919-0_9
3. X.X. Li, D.Y. Cui, C.Y. Zou et al., Assembly-level analysis on temperature coefficient of reactivity in a graphite-moderated fuel salt reactor fueled with low-enriched uranium. Nucl. Sci. Tech. **34**, 70 (2023). https://doi.org/10.1007/s41365-023-01216-0
4. G.A. Wen, J.H. Wu, C.Y. Zou et al., Preliminarysafety analysis for a heavy water-moderated molten salt reactor. Nucl. Sci. Tech. **35**, 106 (2024). https://doi.org/10.1007/s41365-024-01476-4
5. X.C. Zhao, R. Yan, G.F. Zhu et al., Plutonium utilization in a small modular molten-salt reactor based on a batch fuel reprocessing scheme. Nucl. Sci. Tech. **35**, 68 (2024). https://doi.org/10.1007/s41365-024-01428-y
6. X.D. Zuo, M.S. Cheng, Y.Q. Dai et al., Flow field effect of delayed neutron precursors in liquid-fueled molten salt reactors. Nucl. Sci. Tech. **33**, 96 (2022). https://doi.org/10.1007/s41365-022-01084-0
7. L.Y. He, Y. Cui, L. Chen et al., Effect of reprocessing on neutrons of a molten chloride salt fast reactor. Nucl. Sci. Tech. **34**, 46 (2023). https://doi.org/10.1007/s41365-023-01186-3
8. C.Y. Zou, C.G. Yu, J. Zhou et al., Minor actinides transmutation in thermal, epithermal and fast Molten Salt Reactors with very deep burnup. Proceedings of the 23rd Pacific Basin Nuclear Conference, vol. 1 (Singapore, 2023), pp. 656–672. https://doi.org/10.1007/978-981-99-1023-6_57
9. S. Liu, J. Cai, Studies of fuel loading pattern optimization for a typical pressurized water reactor (PWR) using improved pivot particle swarm method. Ann. Nucl. Energy **50**, 117 (2012). https://doi.org/10.1016/j.anucene.2012.08.007
10. R.C. Robertson, MSRE Design and Operations Report. Part I. Description of Reactor Design. Oak Ridge National Lab. ORNL-TM-728 (1965). doi: https://doi.org/10.2172/4654707
11. R. Roper, M. Harkema, P. Sabharwall et al., Molten salt for advanced energy applications: a review. Ann. Nucl. Energy **169**, 108924 (2022). https://doi.org/10.1016/j.anucene.2021.108924

12. Z.M. Dai, Thorium molten salt reactor nuclear energy system (TMSR). Molten Salt Reactors and Thorium Energy 531–540 (2017). https://doi.org/10.1016/B978-0-08-101126-3.00017-8
13. C.A.M. Silva, I.R. Magalhaes, M. Lorduy-Alos et al., A neutronic evaluation of a thorium-based molten salt breeder reactor. Nucl. Eng. Des. **421**, 113049 (2024). https://doi.org/10.1016/j.nucengdes.2024.113049
14. C. Fiorina, M. Aufiero, A. Cammi et al., Investigation of the MSFR core physics and fuel cycle characteristics. Prog. Nucl. Energy **68**, 153 (2023). https://doi.org/10.1016/j.pnucene.2013.06.006
15. V. Ignatiev, O. Feynberg, I. Gnidoi et al., Molten salt actinide recycler and transforming system without and with Th-U support: fuel cycle flexibility and key material properties. Ann. Nucl. Energy **64**, 408 (2024). https://doi.org/10.1016/j.anucene.2013.09.004
16. T. J. Dolan, I. PáZSIT, A. RYKHLEVSKII, et al. Molten Salt Reactors and Thorium Energy (Second Edition). Woodhead Publishing. (2024). https://doi.org/10.1016/B978-0-323-99355-5.00020-3
17. L. Wang, W. Sun, B.Y. Xia et al., Preferred core conceptual design of pebble bed advanced high temperature reactor. Ann. Nucl. Energy **151**, 107983 (2021). https://doi.org/10.1016/j.anucene.2020.107983
18. D. Jiang, D.L. Zhang, X. Li et al., Fluoride-salt-cooled high-temperature reactors: review of historical milestones, research status, challenges, and outlook. Renew. Sustain. Energy Rev. **161**, 112345 (2022). https://doi.org/10.1016/j.rser.2022.112345
19. B.E. Prince, S.J. Ball, J.R. Engel et al., Zero-power physics experiments on the Molten-Salt Reactor experiment. Oak Ridge National Lab. ORNL-4233 (1968). doi: https://doi.org/10.2172/4558029
20. P.N. Haubenreich, J.R. Engel, B.E. Prince et al., MSRE design and operations report. PART III. Nuclear analysis. Oak Ridge National Lab. ORNL-TM-730 (1964). doi: https://doi.org/10.2172/4114686
21. X. Jing, X. Xu, Y. Yang et al., Prediction calculations and experiments for the first criticality of the 10 MW high temperature gas-cooled reactor-test module. Nucl. Eng. Des. **218**, 43 (2022). https://doi.org/10.1016/S0029-5493(02)00184-X
22. A. Bykhun, P. Gladkikh, I. Karnaukhov et al., Reactivity measurement methods and the first results of the physical start-up for the nuclear subcritical facility Neutron Source. Ukr. J. Phys. **68**, 147 (2023). https://doi.org/10.15407/ujpe68.3.147
23. J. Bai, C. Wan, S.G. Hong et al., A practical subcritical rod worth measurement technique based on the improved neutron source multiplication method. Nucl. Eng. Technol. **56**, 1398 (2024). https://doi.org/10.1016/j.net.2023.11.044
24. Y.Q. Shi, Q.F. Zhu, H. Tao, Review and research of the neutron source multiplication method in nuclear critical safety. Nucl. Technol. **149**, 122 (2005). https://doi.org/10.13182/NT05-2
25. R.C. Diniz, F.S. Rosa, A.D.C. Goncalves, Reactivity calculation in molten salt reactors with inverse kinetics model. Ann. Nucl. Energy **194**, 110130 (2023). https://doi.org/10.1016/j.anucene.2023.110130
26. W. Jiang, Q.F. Zhu, Q. Zhou et al., Reactivity worth measurement of the lead target on VENUS-II light water reactor and validation of evaluated nuclear data. Ann. Nucl. Energy **165**, 108779 (2022). https://doi.org/10.1016/j.anucene.2021.108779
27. G. Truchet, W.F.G. Rooijen, Y. Shimazu et al., Application of the modified neutron source multiplication method to the prototype FBR Monju. Ann. Nucl. Energy **51**, 94 (2013). https://doi.org/10.1016/j.anucene.2012.07.040
28. W. Wang, C. Liu, L. Huang, The first application of modified neutron source multiplication method in subcriticality monitoring based on Monte Carlo. Nucl. Eng. Technol. **52**, 477 (2020). https://doi.org/10.1016/j.net.2019.08.014
29. O. Ashraf, G.V. Tikhomirov, Preliminary study on the online reprocessing and refueling scheme for SD-TMS reactor. J. Phys. Conf. Ser. **1439**, 012005 (2020). https://doi.org/10.1088/1742-6596/1439/1/012005
30. S. Xia, J. Chen, W. Guo et al., Development of a Molten Salt Reactor specific depletion code MODEC. Ann. Nucl. Energy **124**, 88–97 (2019). https://doi.org/10.1016/j.anucene.2018.09.032
31. G.F. Zhu, Y. Zou, M.H. Li et al., Development of burnup calculation code for pebble-bed high temperature reactor at equilibrium state. At. Energy Sci. Technol. **49**, 890 (2015). https://doi.org/10.7538/yzk.2015.49.05.0890
32. J.C.B. Fiel, Neutronic calculations of a thermal reactor using the Albedo Method in two energy groups. Ann. Nucl. Energy **115**, 83 (2018). https://doi.org/10.1016/j.anucene.2018.01.002
33. G.J. Janz, Thermodynamic and transport properties for molten salts:correlation equations for critically evaluated density, surface tension, electrical conductance, and viscosity data. J. Phys. Chem. Ref. Data **17**, 311 (1988)
34. D.F. Williams, Assessment of candidate Molten Salt Coolants for the NGNP/NHI heat-transfer loop. Oak Ridge National Lab. ORNL/TM-2006/69 (2006). https://doi.org/10.2172/1360677
35. J. Park, A. Leong, J. Zhang, Density measurements of molten salte. J. Chem. Eng. Data **68**, 1892 (2023). https://doi.org/10.1021/acs.jced.3c00171
36. S.M. Bowman, SCALE 6: Comprehensive nuclear safety analysis code system. Nucl. Technol. **174**, 126 (2011). https://doi.org/10.13182/NT10-163
37. B. Zhou, X.H. Yu, Y. Zou et al., Study on dynamic characteristics of fission products in 2 MW molten salt reactor. Nucl. Sci. Tech. **31**, 17 (2020). https://doi.org/10.1007/s41365-020-0730-z
38. L. Chen, R. Yan, X.Z. Kang et al., Study on the production characteristics of ^{131}I and ^{90}Sr isotopes in a molten salt reactor. Nucl. Sci. Tech. **32**, 33 (2021). https://doi.org/10.1007/s41365-021-00867-1
39. P. Thomas, 21 - Nuclear reactors. Simulation of Industrial Processes for Control Engineers **268**, 81 (1999). https://doi.org/10.1016/B978-075064161-6/50022-5
40. M.L. Tan, G.F. Zhu, Z.D. Zhang et al., Burnup optimization of once-through molten salt reactors using enriched uranium and thorium. Nucl. Sci. Tech. **33**, 5 (2022). https://doi.org/10.1007/s41365-022-00995-2
41. C.Q. Yu, G.F. Zhu, Y.F. Liu et al., Comparative study on the neutronic performance of thermal and Fast Molten Salt Reactors under once-through fuel cycle. Int. J. Energy Res. **12**, 1–18 (2023). https://doi.org/10.1155/2023/8875215
42. S. Marguet, The Physics of Nuclear Reactors. Cham; Springer International Publishing. (2017). https://doi.org/10.1007/978-3-319-59560-3_7
43. X.Z. Kang, G.F. Zhu, J.H. Wu et al., Core optimization for extending the graphite irradiation lifespan in a small modular Thorium-Based Molten Salt Reactor. J. Nucl. Eng. **5**, 16 (2024). https://doi.org/10.3390/jne5020012
44. C.Y. Zou, X.Z. Cai, D.Z. Jiang et al., Optimization of temperature coefficient and breeding ratio for a graphite-moderated molten salt reactor. Nucl. Eng. Des. **281**, 114 (2015). https://doi.org/10.1016/j.nucengdes.2014.11.022

45. M.L. Tan, G.F. Zhu, Y. Zou et al., Research on the effect of the heavy nuclei amount on the temperature reactivity coefficient in a small modular molten salt reactor. Nucl. Sci. Tech. **30**, 9 (2019). https://doi.org/10.1007/s41365-019-0666-3